



Eddy memory in weakly nonlinear two-layer quasi-geostrophic ocean flows

Henk A. Dijkstra^{1,2,a} , Georgy Manucharyan³, Woosok Moon⁴

¹ Institute for Marine and Atmospheric research Utrecht, Department of Physics, Utrecht University, Utrecht, The Netherlands

² Center for Complex Systems Studies, Utrecht University, Utrecht, The Netherlands

³ School of Oceanography, University of Washington, Seattle, WA, USA

⁴ Department of Environmental Atmospheric Sciences, Pukyong National University, 48513 Pusan, South Korea

Received: 3 July 2022 / Accepted: 3 October 2022

© The Author(s) 2022

Abstract In this paper, we study the origin of eddy-memory effects in a weakly nonlinear regime of a baroclinically unstable zonal ocean flow in a zonal channel. In this weakly nonlinear regime, the memory kernel can be analytically derived in case of an externally imposed time-dependent wind-stress forcing. Here, the memory arises because it takes a finite time for the nonlinear flow to equilibrate and the memory kernel is a decaying (in time) exponential function. When there is no external forcing, eddy-memory effects arise due to successive rectification of the background flow which is due to the self-interaction of the unstable modes. While the memory kernel cannot explicitly be calculated in this case, it is also argued to be a decaying exponential function. In both cases, the memory strength is inversely proportional to the growth rate of the instabilities at criticality.

1 Introduction

It has long been recognized that ocean mesoscale eddies modify the basin-scale flows, in particular western boundary currents such as the Gulf Stream in the North Atlantic and the Kuroshio in the North Pacific [1]. This is most clearly seen when large-scale flows are compared in ocean models where the horizontal grid spacing allows for an explicit representation of eddies and those where the grid spacing is too coarse [2, 3]. The mechanisms of the large-scale flow modification are well known and are generally referred to as rectification mechanisms. For example, eddies can give rise to up-gradient momentum transport, thereby enhancing velocities of the background large-scale flows [4].

Parameterizations of the effects of eddies on tracer transports have been crucial for increasing the performance of non-eddy climate models. One of the most implemented parameterizations is the GM scheme [5], which represents the effect of mesoscale eddies on tracers as advection by an eddy overturning streamfunction. The strength of the streamfunction is proportional to the eddy buoyancy fluxes, for which a diffusive closure is used as follows:

$$\overline{\mathbf{v}'b'} = -K_b \nabla \bar{b} \quad (1)$$

where \mathbf{v} is the horizontal velocity field, b the buoyancy field and the prime and bar indicate anomalies and mean, respectively; the parameter K_b is the GM diffusion coefficient. In a layer-thickness formulation [6], a parameterization more in line with diffusion of potential vorticity [7] can be written as

$$\overline{\mathbf{v}'h'} = -K_h \nabla \bar{h} \quad (2)$$

where h now indicates the layer thickness and K_h the layer-thickness diffusion coefficient.

The role of eddies in the large-scale ocean circulation has been extensively studied, in particular in the Southern Ocean [8]. Simulations with strongly eddy ocean models demonstrated that new types of low-frequency variability can occur due to eddy-mean flow or eddy-eddy interactions [9]. Examples are the multi-decadal variability in the Southern Ocean such as found in a multilayer quasi-geostrophic model [10] and in global ocean models [11].

Several studies have proposed to explain low-frequency variability phenomena in strongly eddy ocean models by a ‘memory effect’ of the eddies affecting the large-scale flow. In [12], it is shown that the response of an eddy model to wind forcing does not conform to the GM behavior. There is a decadal timescale phase difference between the variation of the mean eddy-kinetic energy and that of the mean buoyancy field. To explain this phase difference, a new parameterization of the form

$$\overline{\mathbf{v}'h'} = -K_m \int_{-\infty}^t e^{-\frac{t-t'}{\tau}} \nabla \bar{h} dt' \quad (3)$$

^a e-mail: h.a.dijkstra@uu.nl (corresponding author)

was suggested, representing an eddy-memory kernel with a memory timescale r and diffusion coefficient K_m . This parameterization can be also written as

$$\overline{\mathbf{v}'h'} = -K_m \nabla \bar{h}^* \tag{4a}$$

$$\frac{dh^*}{dt} = -\frac{h^*}{r} + \frac{\bar{h}}{r} \tag{4b}$$

where \bar{h}^* carries the memory of \bar{h} . The existence of such a memory component could help explain low-frequency variability phenomena found in eddying ocean models, for example the turbulent oscillator in the midlatitude gyres [9] and the Southern Ocean Mode [11, 13]. Viebahn et al. [14] also show that for a two-level quasi-geostrophic model, the eddy-forcing representation in terms of energy modes improves when a delayed response of these modes is taken into account.

Based on the Mori–Zwanzig approach [15] to multi-scale dynamical systems, one can view representing the effect of the eddies on the large-scale flow as a projection in the state space. Hence, it can introduce a memory kernel in the equations for the large scales [16]. However, the expression in the memory kernel in (3), as suggested in [12], is ad hoc and not based on detailed analysis of the processes giving rise to the memory.

Recently, the effects of eddy memory on the variability of baroclinic atmospheric flows were studied [17, 18]. Using a multiple-scale analysis, the effect of the synoptic scale eddy-heat fluxes on the planetary scale temperature variability showed that the eddy-memory effects modify the character of the planetary temperature equation from parabolic to hyperbolic. This modification leads to an explanation of the dominant intraseasonal mode in the Southern Hemisphere, the baroclinic annular mode [17]. The same modification also allows for new classes of midlatitude planetary waves. Such waves are considered to be relevant to explain atmospheric blocking and/or the effect of polar amplification on the motion of the atmospheric jet [18].

In this paper, our aim is to provide a more detailed view of eddy-memory effects in midlatitude ocean flows, using a model of the weakly nonlinear development of baroclinic instability of a zonal midlatitude jet. Much is known on the linear stability of zonal jets in a horizontally unbounded ocean in the quasi-geostrophic (QG) flow regime. Classical models, such as the Eady model [19] and the Phillips model [20], have led to an understanding of the mechanism of baroclinic instability. Long waves destabilize a zonal jet with maximum growth rates occurring for perturbations having wavelengths on the order of the internal Rossby deformation radius, typically 50 – 100 km in the ocean at midlatitudes. In case linear friction is included, the neutral curve has a minimum at (k_c, μ_c) where k_c is the critical wave number and μ_c the critical value of the control parameter (e.g., the maximum speed of the zonal jet).

The nonlinear development of these perturbations has been extensively analyzed in the weakly nonlinear case [21–24]. In the regime $|k - k_c| = \mathcal{O}(\epsilon)$, $\epsilon \ll 1$, and $|\mu - \mu_c| = \mathcal{O}(\epsilon^2)$, Van der Vaart and Dijkstra [25] showed that on a long timescale $T = \epsilon^2 t$ and large spatial scale $X = \epsilon(x - c_g t)$, where c_g is the group velocity of the waves at criticality, the complex amplitude A of the wave packet destabilizing the jet satisfies a Ginzburg–Landau equation (abbreviated from now as GLE)

$$\frac{\partial A}{\partial T} = \gamma_1 A + \gamma_2 \frac{\partial^2 A}{\partial X^2} - \gamma_3 A|A|^2 \tag{5}$$

where the $\gamma_i \in \mathbb{C}$ are constants. They also showed that the Stokes solution $A(T)$ of this equation can become unstable to sideband instabilities. The GLE will play a key role in identifying the memory kernel induced by the instabilities of the background flow.

In Sect. 2, the quasi-geostrophic model, the linear stability problem and the weakly nonlinear theory is presented. Numerical results for the reference case will be presented in Sec. 3 and will serve as the basis for the eddy-memory analysis in Sect. 4. Here, we first derive the memory kernel in the case of a slowly varying wind stress (Sect. 4.1) and then provide a more heuristic analysis in the case of constant wind forcing (Sect. 4.2). Section 5 provides a summary and a discussion of the results.

2 Formulation

2.1 Model

We consider two layers of homogeneous fluids, with an upper layer density ρ_1 and lower layer density ρ_2 (with $\rho_1 < \rho_2$) and with equilibrium layer thicknesses H_1 and H_2 , respectively. The reduced gravity is indicated by $g' = (\rho_2 - \rho_1)/\rho_0$, where ρ_0 is a reference density. These layers are located in a midlatitude β -plane channel with width $2L$ and with Coriolis parameter $f = f_0 + \beta_0 y$. This flow can be modeled by the two-layer QG model [22] using the geostrophic stream function ψ_i , $i = 1, 2$ and the vertical component of the relative vorticity ζ_i , $i = 1, 2$ in each layer. The quantities ψ_i and ζ_i are non-dimensionalized by UL and U/L , respectively, length with L and time with L/U , where U is a characteristic horizontal velocity.

To be compatible with the results in [25], the non-dimensional equations are written here explicitly as

$$\frac{D_1}{dt}(\nabla^2 \psi_1 + \beta y + F(\psi_2 - \psi_1)) = -\tau_w \frac{\partial \tau^x}{\partial y} - r_0 \nabla^2 \psi_1 \tag{6a}$$

$$\frac{D_2}{dt}(\nabla^2 \psi_2 + \beta y - F\delta(\psi_2 - \psi_1)) = -\tau_w \alpha \frac{\partial \tau^x}{\partial y} - r_0 \nabla^2 \psi_2 \tag{6b}$$

where τ^x is the zonal wind stress at the surface and $\alpha\tau^x$ is the interfacial stress on the interface between the two layers, where $\alpha = U_2/U_1$ is the ratio of the maximal dimensional velocities in the layers. The latter term is needed to be consistent with having linear friction terms in both layers [25]. The dimensionless parameters are the layer-thickness ratio $\delta = H_1/H_2$, the Froude number $F = f_0^2 L^2 / (g' H_1)$ and the linear friction coefficient r_0 . Furthermore, $\beta = \beta_0 L^2 / U$ is the planetary potential vorticity gradient and τ_w is a measure of the wind-stress amplitude. The operators $D_i/dt, i = 1, 2$ are the material derivatives in each layer.

We will consider the stability of a general zonal jet [25] with

$$\bar{\psi}_1 = -\Psi(y; v); \quad \bar{\psi}_2 = -\alpha\Psi(y; v) = \alpha\bar{\psi}_1 \tag{7}$$

on the domain $y \in [-1, 1]$, The function $\Psi(y; v)$ defines the meridional profile of the jet and v is a non-dimensional measure of its width. By construction, this is a steady solution of the model equations (6b) when the background wind stress $\bar{\tau}^x$ satisfies

$$\frac{\partial \bar{\tau}^x}{\partial y} = \frac{r_0}{\tau_w} \nabla^2 \bar{\psi}_1 \tag{8}$$

from which it can be determined up to an additive constant; the explicit expression for $\bar{\tau}^x$ is not important here.

By considering the perturbations $\phi_i = \psi_i - \bar{\psi}_i, i = 1, 2$, we can write the non-dimensional equations governing the evolution of the perturbations in the following operator form [25], using $\Phi = (\phi_1, \phi_2)$,

$$\left(\mathcal{M} \frac{\partial}{\partial t} + \mathcal{L}\right)\Phi + \mathcal{N}(\Phi)\Phi = 0 \tag{9}$$

Here \mathcal{M}, \mathcal{L} and \mathcal{N} are the operators defined as

$$\mathcal{M} = \begin{pmatrix} \nabla^2 - F & F \\ \delta F & \nabla^2 - \delta F \end{pmatrix} \tag{10a}$$

$$\mathcal{L} = \begin{pmatrix} \bar{u} \frac{\partial}{\partial x} (\nabla^2 - F) + \Pi'_1 \frac{\partial}{\partial x} + r_0 \nabla^2 & \bar{u} F \frac{\partial}{\partial x} \\ \bar{u} \alpha \delta F \frac{\partial}{\partial x} & \alpha \bar{u} \frac{\partial}{\partial x} (\nabla^2 - \delta F) + \Pi'_2 \frac{\partial}{\partial x} + r_0 \nabla^2 \end{pmatrix} \tag{10b}$$

$$\mathcal{N}(\Phi) = \begin{pmatrix} \left(\frac{\partial \phi_1}{\partial x} \frac{\partial}{\partial y} - \frac{\partial \phi_1}{\partial y} \frac{\partial}{\partial x}\right) (\nabla^2 - F) & F \left(\frac{\partial \phi_1}{\partial x} \frac{\partial}{\partial y} - \frac{\partial \phi_1}{\partial y} \frac{\partial}{\partial x}\right) \\ \delta F \left(\frac{\partial \phi_2}{\partial x} \frac{\partial}{\partial y} - \frac{\partial \phi_2}{\partial y} \frac{\partial}{\partial x}\right) & \left(\frac{\partial \phi_2}{\partial x} \frac{\partial}{\partial y} - \frac{\partial \phi_2}{\partial y} \frac{\partial}{\partial x}\right) (\nabla^2 - \delta F) \end{pmatrix} \tag{10c}$$

with $\bar{u} = \Psi'$ and where the potential vorticity gradients Π'_i are given by

$$\Pi'_1 = \beta + F(1 - \alpha)\bar{u} - \bar{u}'' \tag{11a}$$

$$\Pi'_2 = \beta - \delta F(1 - \alpha)\bar{u} - \bar{u}'' \tag{11b}$$

2.2 Linear stability analysis

The linear stability problem (where nonlinear interactions of the perturbations are neglected) is formulated as

$$\left(\mathcal{M} \frac{\partial}{\partial t} + \mathcal{L}\right)\tilde{\Phi} = 0 \tag{12}$$

for infinitesimally small perturbations $\tilde{\Phi}$.

As the x -direction is unbounded, traveling wave solutions of (12) exist with wave number k and complex growth factor σ , i.e.,

$$\tilde{\Phi}(x, y, t) = \hat{\Phi}(y)e^{ikx + \sigma t} + c.c. \tag{13}$$

where $c.c.$ indicates complex conjugate. Substitution of (13) into (12) gives a boundary value problem for the eigenpair $(\sigma, \hat{\Phi})$, i.e.,

$$(\hat{\mathcal{M}}(k)\sigma + \hat{\mathcal{L}}(k))\hat{\Phi} = 0 \tag{14}$$

with appropriate boundary conditions. Here the operators $\hat{\mathcal{M}}$ and $\hat{\mathcal{L}}$ are the Fourier transforms of the original operators \mathcal{M} and \mathcal{L} in the x -direction, respectively.

The eigenvalue is written as $\sigma = \lambda + i\omega$ and considered as a function of the wave number k and the control parameter μ . The neutral curve $\lambda(k, \mu) = 0$ provides sufficient conditions for instability, and in the examples considered below, the neutral curve has a minimum at (k_c, μ_c) at which

$$\lambda(k_c, \mu_c) = 0; \quad \frac{\partial \lambda}{\partial k}(k_c, \mu_c) = 0; \quad \frac{\partial^2 \lambda}{\partial k^2}(k_c, \mu_c) < 0 \tag{15}$$

Below we will use the notation $\omega_c = \omega(k_c)$.

2.3 Weakly nonlinear analysis

Assume now conditions just above criticality, i.e.,

$$\mu = \mu_c + m\epsilon^2, \quad (16)$$

where $\epsilon \ll 1$ and $m = \mathcal{O}(1)$. As the neutral curve can be approximated by a parabola $\mu - \mu_c \sim (k - k_c)^2$, this implies that $|k - k_c| = \mathcal{O}(\epsilon)$. The unstable traveling waves are hence limited to a narrow band around k_c which can be interpreted as a wave packet with central wave number k_c . This wave packet evolves on a timescale which is large compared to typical wave periods $2\pi/\omega$ and is characterized by scales

$$T = \epsilon^2 t; \quad X = \epsilon(x - c_g t) \quad (17)$$

where $c_g = \partial\omega/\partial k$ is the group velocity. The long spatial variable X is a slowly moving coordinate, traveling with the group velocity of the growing wave packet.

The scaling leads to transformations for $\Phi(x, X(x, t), y, t, T(t))$ as

$$\frac{\partial}{\partial t} \rightarrow \frac{\partial}{\partial t} - \epsilon c_g \frac{\partial}{\partial X} + \epsilon^2 \frac{\partial}{\partial T} \quad (18a)$$

$$\frac{\partial}{\partial x} \rightarrow \frac{\partial}{\partial x} + \epsilon \frac{\partial}{\partial X} \quad (18b)$$

The final amplitude of the perturbations will be small compared to that of the background state, for μ close to μ_c , so the solution vector is expanded in terms of the small parameter ϵ and Fourier modes of the marginally stable wave $E = \exp(i(k_c x + \omega_c t))$, i.e.,

$$\Phi = \epsilon \Phi^{(11)} E + \epsilon^2 (\Phi^{(02)} + \Phi^{(12)} E + \Phi^{(22)} E^2) + \epsilon^3 \Phi^{(13)} E + \dots + c.c. \quad (19)$$

where the $\Phi^{(ij)} = \Phi^{(ij)}(X, y, T)$ depend on the slow timescale and long spatial scale.

Substitution of (19) into (9) and collecting terms of the same order (in ϵ and E) give at $\mathcal{O}(\epsilon E)$ the linear stability problem

$$(i\omega_c \hat{\mathcal{M}}(k_c) + \hat{\mathcal{L}}(k_c)) \Phi^{(11)} = 0 \quad (20)$$

As the left-hand side does not operate on the large scales X and T , we can write $\Phi^{(11)} = A(X, T)\Psi$, where $\Psi = \hat{\Phi}(y)$ is the eigenvector at $k = k_c$ from (14). The weakly nonlinear analysis eventually (see Appendix) leads to a GLE for the scalar (but complex) amplitude $A(X, T)$, i.e.,

$$\frac{\partial A}{\partial T} = \gamma_1 A + \gamma_2 \frac{\partial^2 A}{\partial X^2} - \gamma_3 A|A|^2 \quad (21)$$

where the γ_i , $i = 1, 2, 3$ are three (in general) complex numbers.

The solutions of the GLE capture the weakly nonlinear interactions just above criticality in the flow. The weakly nonlinear problem, including determining the coefficients of the GLE, is solved by expanding the functions ϕ_i , $i = 1, 2$ into Chebyshev polynomials and the procedure is described in detail in [25]. The only numerical parameter in this approach is the number of Chebyshev polynomials taken into account, which we will indicate below by n_C .

3 Results: weakly nonlinear flow development

The weakly nonlinear flow development consists of two basic processes: (i) initial (in general oscillatory) exponential growth of the critical mode (the eigenvector at criticality) on a timescale t and (ii) a nonlinear equilibration on a long timescale $T = \epsilon^2 t$. In addition, secondary instabilities such as Benjamin–Feir (or sideband) instabilities [25] may occur, which we will not consider below. The value of $n_C = 121$ was taken in all results presented here, which was shown in [25] to give sufficient accuracy in all quantities computed.

We discuss the reference case [25] in quite detail in this section, as it is central for the eddy-memory analysis in the next section. The background jet for the reference case is:

$$\bar{u}_1(y) = -\Psi'(y; \nu) = 1 - \frac{\tanh^2(\frac{y}{\nu})}{\tanh^2(\frac{1}{\nu})} \quad (22a)$$

$$\bar{u}_2(y) = \alpha \bar{u}_1(y) \quad (22b)$$

where $\nu = 0.3$ and $\alpha = 0.22$. A plot of this background zonal velocity is shown on the domain $y \in [0, 1]$ in Fig. 1 with maximal velocities occur in the jet center.

Just as in [25], we take $\mu = \beta^{-1}$ as the control parameter and fix the other parameters as $F = 13.2$, $\delta = 0.22$ and $r_0 = 0.4$. The neutral curve, resulting from the linear stability analysis of (22) is plotted in Fig. 2a and shows that the minimum is obtained at

Fig. 1 Background zonal jet in both layers for the reference case [25] with parameters $\nu = 0.3$ and $\alpha = 0.22$

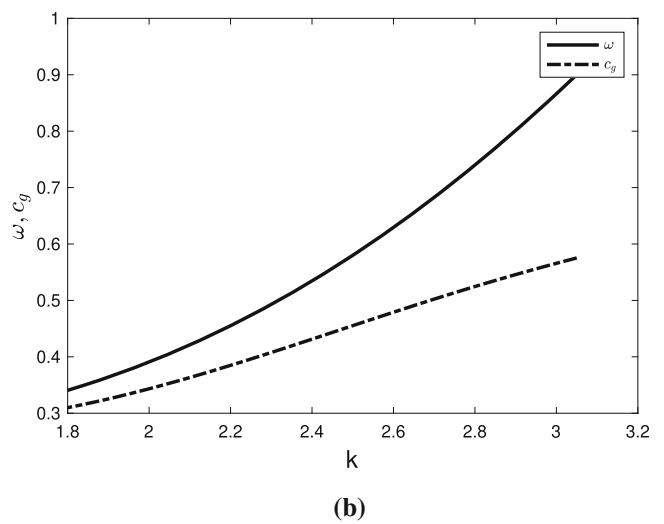
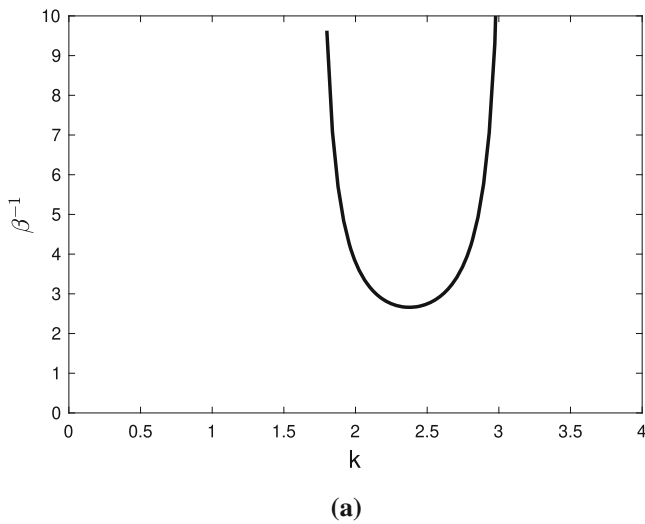
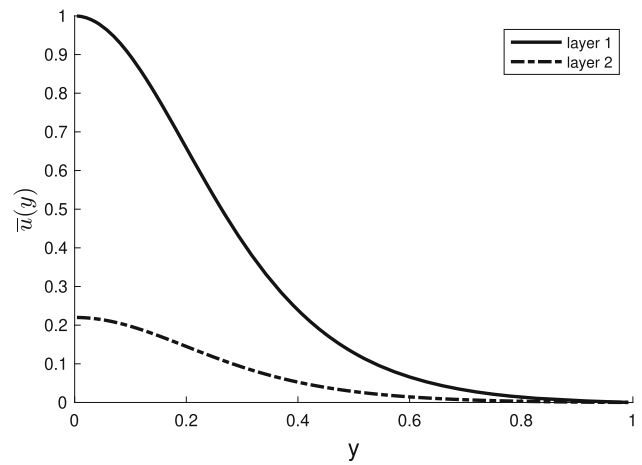


Fig. 2 **a** Neutral curve from the linear stability analysis of the zonal jet in the reference case, where k is the wave number and $\mu = \beta^{-1}$ is used as a control parameter. **b** Frequency and group velocity of the marginally stable mode versus the wave number k

$(k_c, \mu_c) = (2.38, 2.67)$. The frequency ω and group velocity c_g along the neutral curve are shown in Fig. 2b and are monotonically increasing with k ; the critical frequency $\omega_c = 0.52$.

The real and imaginary parts of the zonal (u_j^R and u_j^I) and meridional (v_j^R and v_j^I) velocity perturbations at each layer j of the critical mode are plotted in Fig. 3. Note that the zonal velocity perturbations are odd functions (with respect to $y = 0$) in y and those of the meridional velocity perturbations are even functions in y . The patterns of the actual (dimensionless) velocity perturbations can be obtained from (with \mathcal{R} indicating the real part)

$$u_j(x, y, t) = 2\mathcal{R}((u_j^R + i u_j^I)e^{i(k_c x + \omega_c t)}) \tag{23a}$$

$$v_j(x, y, t) = 2\mathcal{R}((v_j^R + i v_j^I)e^{i(k_c x + \omega_c t)}) \tag{23b}$$

and give the typically ‘banana’-shaped patterns in both layers (not shown here) characteristic for baroclinic instability [25].

The weakly nonlinear analysis provides the coefficients of the GLE (56) for the reference case, resulting in

$$\gamma_1 = 0.060669 - i 0.10058 ; \quad \gamma_2 = -0.047020 - i 0.11880 ; \quad \gamma_3 = 5.9721 - i 59.420 \tag{24}$$

and hence

$$\alpha_1 = 2 \frac{\gamma_2^I}{\gamma_2^R} = 2.52 ; \quad \alpha_2 = \frac{\gamma_3^I}{\gamma_3^R} = -9.9496 \tag{25}$$

which is in agreement with the results in [25], who calculated $\alpha_1 = 2.51$ and $\alpha_2 = -9.76$. The small difference is due to the slightly different singular value decomposition routine used here compared to that in [25].

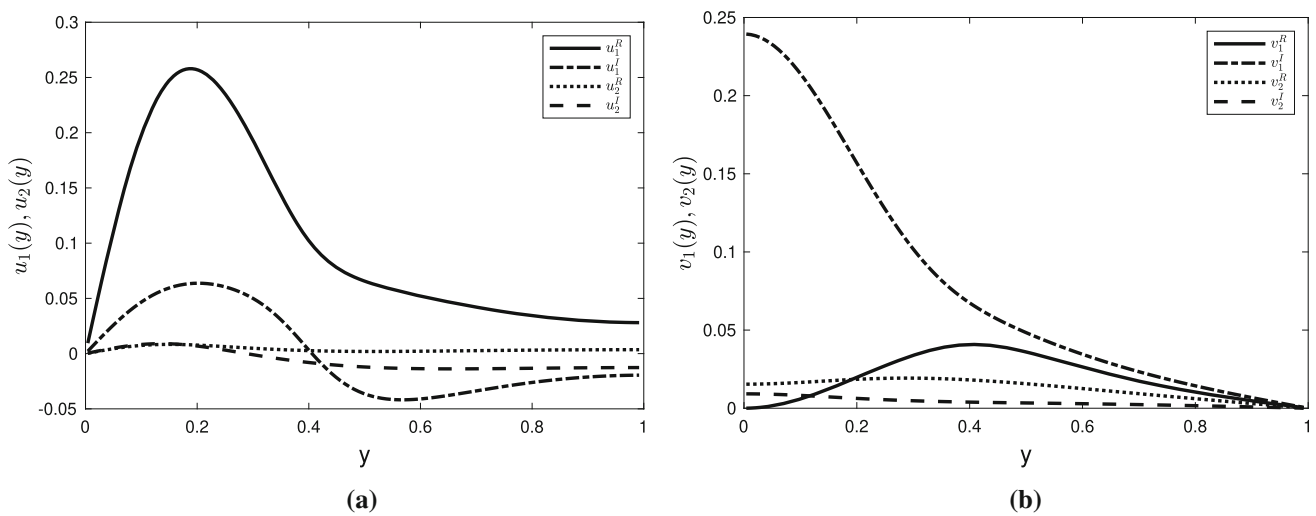


Fig. 3 **a** Distributions of the real and imaginary parts of the zonal velocity of the critical mode in both layers. **b** Distributions of the real and imaginary parts of the meridional velocity of the critical mode in both layers

A special solution of the Ginzburg–Landau equation is the so-called Stokes solution, where the amplitude A is only a function of T and hence has no spatial dependence. This solution is given by

$$A(T) = A_s e^{i\Omega T} \tag{26}$$

and we find from (5)

$$|A_s|^2 = \frac{\gamma_1^R}{\gamma_3^R} \tag{27a}$$

$$\Omega = \gamma_1^I - \gamma_3^I |A_s|^2 \tag{27b}$$

Hence, when starting from an arbitrary initial condition and a parameter regime with a stable Stokes solution, then the equilibrium solution will oscillate with a frequency Ω and approach a steady amplitude with value $|A_s|$. Such behavior is, for example, shown in Fig. 13a of Van der Vaart and Dijkstra [25].

In fact, the evolution equation for the amplitude $|A|^2$ can be written as

$$\frac{d|A|^2}{dT} = 2\gamma_1^R |A|^2 - 2\gamma_3^R |A|^4 \tag{28}$$

where $\gamma_i^R = \mathcal{R}(\gamma_i)$. This is a Bernoulli equation having a solution

$$|A|^2(T) = \left(\frac{\gamma_3^R}{\gamma_1^R} (1 - e^{-2\gamma_1^R T}) + \frac{1}{|A_0|^2} e^{-2\gamma_1^R T} \right)^{-1} \tag{29}$$

where $A(T = 0) = A_0$. The solution $|A|^2(T)$ is shown for the reference case in Fig. 4 for three values of A_0 . There is exponential growth on short timescales T , proportional to the second term in (29), i.e., $|A|^2(T) \sim |A_0|^2 e^{2\gamma_1^R T}$, which is followed by equilibration for larger T according to the first term, where $|A|^2(T) \sim \frac{\gamma_1^R}{\gamma_3^R} (1 - e^{-2\gamma_1^R T})^{-1}$, independent of A_0 . For $T \rightarrow \infty$, the solution $|A|^2(T) \rightarrow \gamma_1^R / \gamma_3^R = |A_s|^2$ (~ 0.01 for the reference case).

The weakly nonlinear theory provides a way to determine nonlinear equilibrium solutions due to the interaction of instabilities with the background state. To determine how far one can go from the critical point, the growth rate near the critical point is expanded as

$$\lambda(k, \mu) \sim \lambda(k_c, \mu_c) + (\mu - \mu_c) \frac{\partial \lambda}{\partial \mu}(k_c, \mu_c) = m \epsilon^2 \frac{\partial \lambda}{\partial \mu}(k_c, \mu_c) \tag{30}$$

Since growth rates of $\mathcal{O}(\epsilon^2)$ are only able to balance the weakly nonlinear interactions on the long timescale T , we choose, with the notation $\lambda_\mu^c = \partial \lambda / \partial \mu(k_c, \mu_c)$,

$$m = (\lambda_\mu^c)^{-1} \tag{31}$$

Fig. 4 Solution of $|A|^2(T)$ for the Stokes solution of the Ginzburg–Landau equation for three different values of A_0 and parameters of the reference case

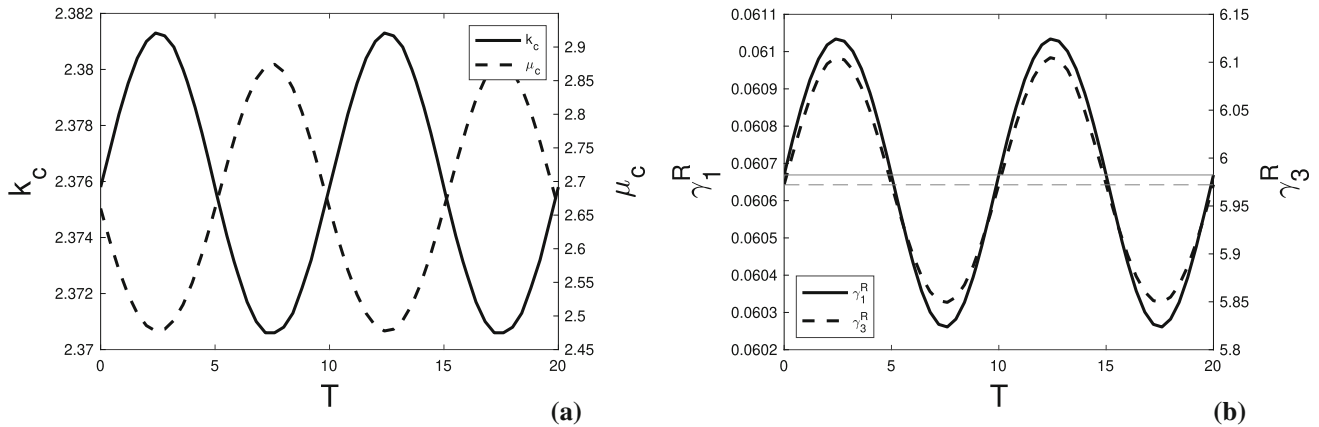
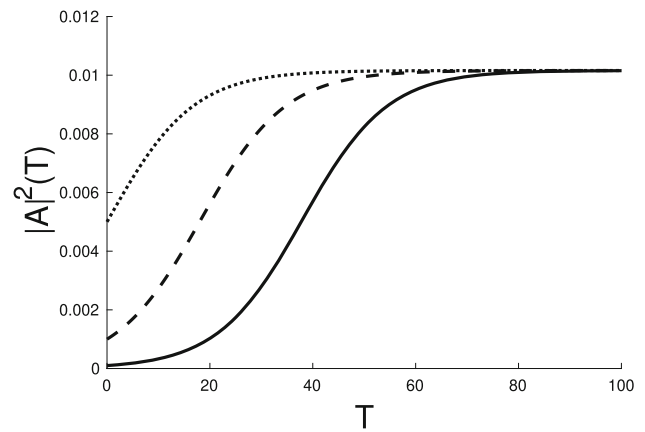


Fig. 5 a Change in the coefficients k_c and μ_c with T . **b** Change of γ_1^R and γ_3^R with the forcing (33) for $T_m = 20$, $\omega_0 = \pi/T_m$ and $\eta = 0.01$

With $\delta = (\mu - \mu_c)/\mu_c$, we find that ϵ is determined from

$$\epsilon = \sqrt{\delta \mu_c \lambda_\mu^c} \tag{32}$$

For a value $\delta = 0.1$, we find for the reference case that $\epsilon = 0.047$, and for $\delta = 1$, we find for this case that $\epsilon = 0.15$. Note that time T is scaled with $L/(U\epsilon^2)$, so one unit T for $\delta = 1$ corresponds to about 50 days (with $L = 10^5$ m and $U = 1$ ms⁻¹). The dimensionless growth timescale in (29) hence corresponds to $T_e = 1/(2\gamma_1^R) = 8.3$ which is about 420 days for the reference case.

4 Eddy memory

Having found the nonlinear equilibrium solution just above criticality, we can now turn to determining the eddy-memory kernel. We will consider two cases: (i) through an external time-dependent forcing in the wind stress (Sect. 4.1) and (ii) by considering the rectification of the background flow without time-varying external forcing (Sect. 4.2).

4.1 External forcing

We consider the wind stress τ^x to vary on the slow timescale T according to

$$\tau^x(y, T) = \bar{\tau}^x(y)(1 + \eta f(T)) \tag{33}$$

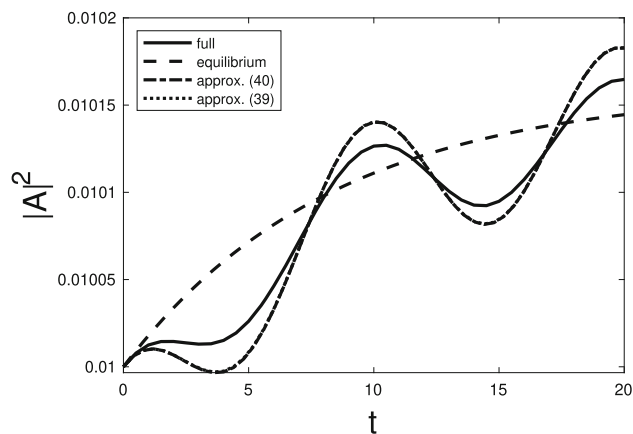
where $f(T)$ describes the time-dependent part and η is a small parameter. According to (8), this time-dependent wind stress will give a time-dependent zonal velocity field \bar{u}_1 and \bar{u}_2 with the same time dependence, i.e.,

$$\bar{u}_1(y, T) = \bar{u}_1^B(y)(1 + \eta f(T)) \tag{34a}$$

$$\bar{u}_2(y, T) = \alpha \bar{u}_1(y, T) = \bar{u}_2^B(y)(1 + \eta f(T)) \tag{34b}$$

where the superscript B refers to the time-independent background velocity used in the previous section.

Fig. 6 Different approximations of the solution of the non-autonomous Ginzburg–Landau equation (35)



As the timescale of the forcing is much larger than that of the growth rate of the instabilities, the time dependence will lead to slowly varying coefficients $\gamma_1^R(T) = \bar{\gamma}_1^R + \eta g_1(T)$ and $\gamma_3^R(T) = \bar{\gamma}_3^R(T) + \eta g_3(T)$ following the weakly nonlinear analysis of Sect. 2. For small η , this leads to the following equation for the amplitude $|A|^2(T)$

$$\frac{d|A|^2}{dT} = 2\gamma_1^R(T)|A|^2 - 2\gamma_3^R(T)|A|^4 \tag{35}$$

which describes the case where small modulations in the forcing on the long timescale T modify the growth and equilibration of the amplitude of the unstable mode. The solution of the equation (35) can be explicitly written as

$$|A|^2(T) = \frac{e^{-h(T)}}{A_0^{-2} + 2 \int_0^T e^{-h(T')} \gamma_3^R(T') dT'} \tag{36a}$$

$$h(T) = -2 \int_0^T \gamma_1^R(T') dT' \tag{36b}$$

This shows that the amplitude $|A|^2(T)$ in general will depend on the history of the forcing through the coefficients γ_i^R . We can make this more explicit by considering a specific example $f(T) = \sin \omega_0 T$ with $\eta = 0.01$ over the interval $T \in [0, T_m]$. The variation in k_c , μ_c and the γ_i^R with T is shown in Fig. 5.

The variation in γ_1^R with respect to $\bar{\gamma}_1^R$ is relatively small (0.6%) compared to that in γ_3^R with respect to $\bar{\gamma}_3^R$ (2.2%) and $g_3(T)$ is in phase with $f(T)$. Under the approximation that $\gamma_1^R \sim \bar{\gamma}_1^R$, the solution $|A|^2(T)$ can be written as

$$|A|^2(T) = (A_0^{-2} e^{-2\bar{\gamma}_1^R T} + 2 \int_0^T e^{-2\bar{\gamma}_1^R(T-T')} \gamma_3^R(T') dT')^{-1} \tag{37}$$

and using $\gamma_3^R(T) = \bar{\gamma}_3^R(1 + \xi f(T))$ we eventually find

$$|A|^2(T) = \frac{|\bar{A}|^2(T)}{1 + 2\xi \bar{\gamma}_3^R |\bar{A}|^2(T) \int_0^T e^{-2\bar{\gamma}_1^R(T-T')} f(T') dT'} \tag{38}$$

where $|\bar{A}|^2(T)$ is the solution for the constant $\bar{\gamma}_i^R$. The last expression explicitly shows (in this limit) the memory integral involving the forcing.

With the further simplification that η (and hence ξ) is so small that the second term in the denominator is much smaller than 1, the final expression becomes

$$|A|^2(T) - |\bar{A}|^2(T) \sim -2\xi \bar{\gamma}_3^R |\bar{A}|^4(T) \int_0^T e^{-2\bar{\gamma}_1^R(T-T')} f(T') dT' \tag{39}$$

which shows that the deviation from the reference case can be written as a convolution integral over the forcing. The memory strength is given by $r = 1/2\bar{\gamma}_1^R$. In the special case that $f(T') = \sin \omega_0 T'$, the explicit expression becomes

$$|A|^2(T) - |\bar{A}|^2(T) \sim -2\xi \bar{\gamma}_3^R |\bar{A}|^4(T) \frac{e^{-2\bar{\gamma}_1^R T} \omega_0 + 2\bar{\gamma}_1^R \sin \omega_0 T - \omega_0 \cos \omega_0 T}{4(\bar{\gamma}_1^R)^2 + \omega_0^2} \tag{40}$$

The numerical solution to (35) for $A_0^2 = 0.01$ is shown as the drawn curve in Fig. 6 and as expected displays a small oscillation around the equilibrium solution for constant $\gamma_i^R = \bar{\gamma}_i^R$ (dashed curve in Fig. 6). The approximate solution (40) is shown as the dash-dotted curve and coincides with the dotted curve displaying the solution (38). The solution (40) is a good approximation to the

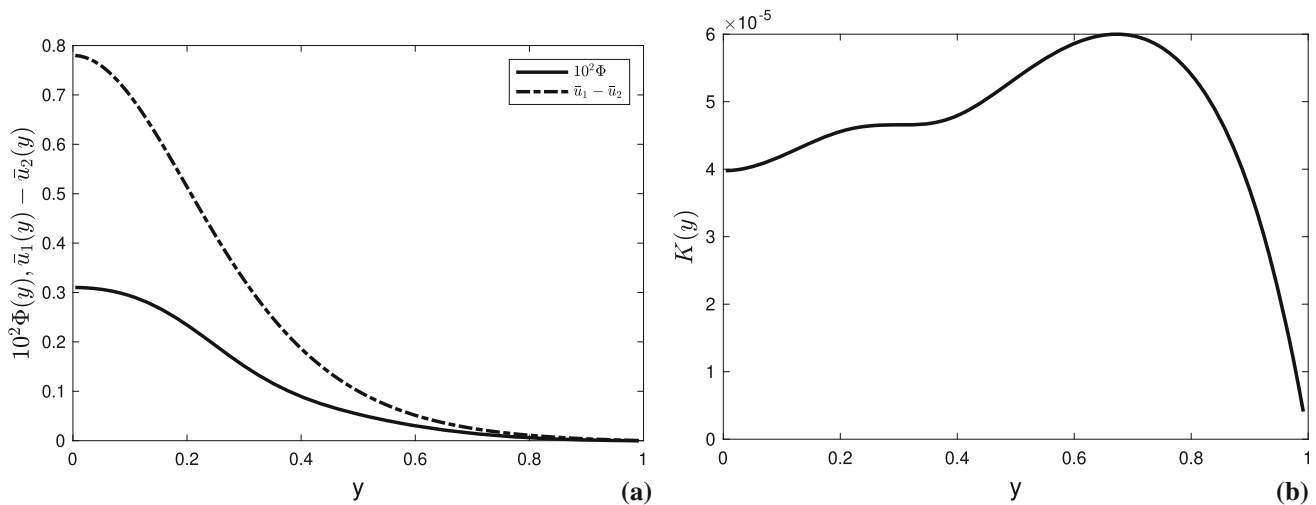


Fig. 7 a Meridional pattern of the thickness flux $\Phi = \overline{v_1^{(11)} h_1^{(11)}}$, i.e., $\bar{\phi}(y) = \mathcal{R}(ik_c \phi_1(\phi_1 - \phi_2)^* - (ik_c \phi_1)^*(\phi_1 - \phi_2))$ and of $\bar{u}_1^B - \bar{u}_2^B$. **b** Coefficient $K(y) = \epsilon^2 \bar{\phi}(y) / (\bar{u}_1^B(y) - \bar{u}_2^B(y))$

full solution, but differs mostly because γ_1^R is not a constant. The phase difference between forcing and solution is caused by the nonlinear interactions (through the term $\xi \bar{\gamma}_3^R$) and also proportional to ω_0 .

To connect to the eddy-thickness flux response to the time-dependent basic state zonal velocity field (which is directly linked to changes in the forcing), we choose the eddy-thickness flux in the first layer $\Phi \equiv \Phi_1$ as observable. This eddy-thickness flux can be directly computed from the Stokes solution, i.e.,

$$\Phi(y, T) = \overline{v_1^{(11)} h_1^{(11)}} = \epsilon^2 |A(T)|^2 \bar{\phi}(y) \tag{41}$$

with $\phi(y) = \mathcal{R}(v_1 h_1^* + v_1^* h_1)(y)$, $v_1 = ik_c \phi_1$ and $h_1 = \phi_1 - \phi_2$, where all these functions are computed at criticality. For the reference case, the spatial structure of $\phi(y)$ is plotted in Fig. 7a together with the vertical shear $\bar{u}_1 - \bar{u}_2$ in the reference case, showing that they have a similar shape. The function $\phi(y)$ is maximal at the midaxis of the jet as is the vertical shear of the background flow.

In the eddy-memory representation, the eddy-thickness fluxes which arise through the interaction of the perturbations with the mean flow can be written as

$$\Phi(y, T) = -K \frac{\partial}{\partial y} \int_{-\infty}^T \kappa(T - T') \bar{h}_1(y, T') dT' = K \int_{-\infty}^T \kappa(T - T') (\bar{u}_1 - \bar{u}_2)(y, T') dT' \tag{42}$$

where κ is the memory kernel with $\kappa(T) = 0$ for $T < 0$ due to causality. Furthermore, \bar{h}_1 is the background layer thickness and K a ‘diffusion’ constant. This implies that the current eddy-thickness fluxes (at time T) depend on the past behavior of the background layer thicknesses.

Under the external forcing, the functions $\phi(y)$ at criticality only vary marginally, and hence (like γ_1^R), we assume that they are equal to that at the reference case $\bar{\phi}(y)$, as shown in Fig. 7a. When considering the additional thickness flux due to the oscillatory component in the time-dependent forcing, i.e.,

$$\Delta \Phi(y, T) = \epsilon^2 (|A(T)|^2 - |\bar{A}(T)|^2) \bar{\phi}(y) \tag{43}$$

we see that $K(y)$ is actually a function defined by

$$K(y) = C \epsilon^2 \frac{\bar{\phi}(y)}{\bar{u}_1^B - \bar{u}_2^B} \tag{44}$$

where $\bar{u}_1 - \bar{u}_2$ is the velocity difference of the steady-state background flow (hence for $\eta = 0$) and C is a constant; this expression (for $C = 1$) is plotted in Fig. 7b. The function $K(y)$ is fairly constant at the middle of the jet but falls off sharply toward the boundaries. In this interpretation of eddy-memory effects in the weakly nonlinear limit, the background flow varies over a long timescale T , and because the instabilities also equilibrate over this timescale, the eddy-thickness flux depends on the history of the background flow.

4.2 Eddy memory: rectification

We next consider the case that the wind stress does not change, but eddy memory can still occur because the stability behavior of the jet changes when it is corrected by instabilities due to rectification.

Fig. 8 Rectification patterns $u_j^{(02)}(y)$ for $j = 1, 2$ of the background zonal velocity due to self-interactions of the critical mode for the reference case. Note that the rectification of the meridional background velocity is zero

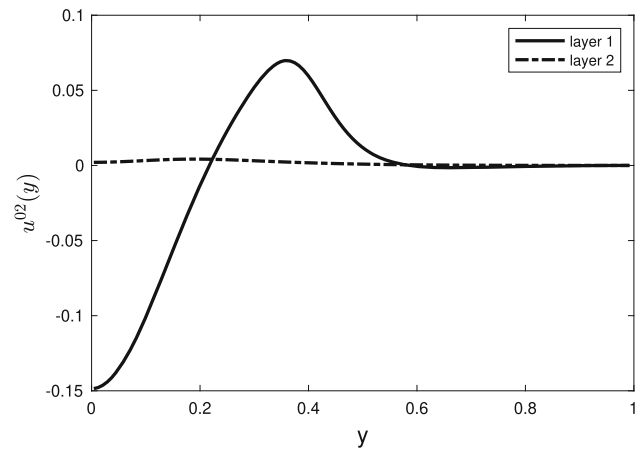
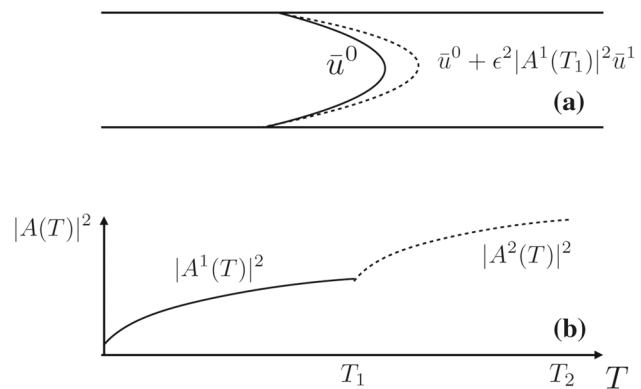


Fig. 9 Sketch of the procedure to determine the memory kernel. **a** Change of the jet due to nonlinear self-interactions of the instabilities. **b** Evolution of the amplitude function $|A^\ell(T)|^2$ over the long timescale T



As is shown in Appendix, the weakly nonlinear analysis leads to a correction to the background zonal flow according to (51cb), with

$$u_j^c(X, y, T) = \epsilon^2 |A|^2(X, T) u_j^{(02)}(y) \tag{45}$$

and the fields $u_j^{(02)}(y)$ at criticality are plotted for the reference case in Fig. 8; note that $v_j^{(02)}(y) = 0$. The correction to the jet in the upper layer has its maximum further away from the central axis compared to that in the lower layer. In the upper layer, the jet is weakened in the center and amplified near $y = 0.4$ which leads to less horizontal shear in the background state. In the lower layer, the jet is strengthened over the whole domain. Hence, this influences the vertical shear of the background flow.

The zonal velocity of the total (weakly nonlinear) Stokes solution at the long timescale T is hence given by

$$\bar{U}_j(x, y, t; T) = \bar{u}_j(y) + \epsilon A(T) u_j^{(11)}(y) e^{i(k_c x + \omega_c t)} + \epsilon^2 |A(T)|^2 u_j^{(02)}(y) \tag{46}$$

and there is also a component which varies on the short space and fast timescales. However, this component averages to zero when zonally averaged and hence is not expected to influence the subsequent secondary instabilities of the jet. The subsequent modifications of the background state (and hence of the background thicknesses \bar{h}_j) will determine the eddy-thickness fluxes at the current time.

To determine the response of the eddy-thickness fluxes to the changing background state over the interval $[T_0, T_1]$, one proceeds as follows (Fig. 9):

- (1) Divide the interval $[T_0, T_1]$ into N discrete intervals with $dT = (T_1 - T_0)/N$.
- (2) At $T_0 = 0$, determine $\gamma_1^1, \gamma_2^1, \gamma_3^1$ and the Stokes solution $|A(T)|^2$, with initial conditions $|A(0)|^2$. Start with $\ell = 1$.
- (3) Over the interval $[(\ell - 1)dT, \ell dT]$, the eddy-thickness fluxes Φ and the background state correction $\bar{u}_j^\ell, j = 1, 2$ can be computed.
- (4) At time $T_\ell = \ell dT$, the stability of the new background state at that time is determined, giving new values of $\gamma_1^{\ell+1}, \gamma_2^{\ell+1}, \gamma_3^{\ell+1}$. Increase ℓ by 1 and go to step (3) until $\ell = N$.
- (5) At time $T_N = \tau = NdT$, determine the $\Phi^N(y)$ in which the memory arises through the variation of the Stokes solution amplitude and the pattern of the background state with time.

Due to the successive modifications of the background state, one can also determine the eddy memory just due to these modifications. Indicate the eddy-thickness fluxes at $T = T_\ell$ as Φ_j^ℓ . Next, we focus only on the upper layer eddy-thickness flux $\Phi^1 = \Phi$ (at $T = T_1$), $\bar{h} = \bar{h}_1$ and $\bar{u} = \bar{u}_1$. First, Φ^1 can only depend on $\bar{h}^0 = \bar{\psi}_1 - \bar{\psi}_2$ (e.g., the thermocline of the background zonal flow) through

$$\Phi^1 = -K \frac{\partial \bar{h}^0}{\partial y} \tag{47}$$

At $T = T_2$, the background jet in the upper layer has been corrected as

$$\bar{u} = \bar{u}^0 + \epsilon^2 |A^1(T_1)|^2 \bar{u}^1; \bar{u}^1 = u_1^{(02)},$$

and hence,

$$\Phi^2 = -K \frac{\partial}{\partial y} (\bar{h}^0 + \epsilon^2 |A^1(T_1)|^2 \bar{h}^1)$$

The difference with the previous section is now that the modification of the background state is proportional to $A^1(T) \sim e^{2\gamma_1^R T}$ and hence, the stability of the background has already changed before this amplitude has equilibrated. Hence, one needs to consider the early stages of growth of the instability where $A^1(T) \sim e^{2\gamma_1^R T}$, and γ_1^R is the value of γ_1^R found during the first step. In this case, we can approximate Φ^2 as

$$\Phi^2 \sim e^{2\gamma_1^R T_1} \frac{\partial}{\partial y} (\bar{h}^0 e^{-2\gamma_1^R T_1} + \epsilon^2 \bar{h}^1)$$

which shows already the memory component of the background state. At $T = T_1$, the background gets corrected again by the Stokes wave and becomes

$$\bar{u} = \bar{u}^0 + \epsilon^2 |A^1(T_1)|^2 \bar{u}^1 + \epsilon^2 |A^2(T_2)|^2 \bar{u}^2,$$

and hence, Φ^3 can be written as (using γ_1^{2R} as the next value of γ_1^R)

$$\Phi^3 \sim e^{2\gamma_1^{2R} T_2} \frac{\partial}{\partial y} (\bar{h}^0 e^{-2\gamma_1^{2R} T_2} + \epsilon^2 (e^{2\gamma_1^{1R} T_1 - 2\gamma_1^{2R} T_2} \bar{h}^1 + \bar{h}^2))$$

which reduces when $\gamma_1^{2R} \sim \gamma_1^{1R}$ to

$$\Phi^3 \sim e^{2\gamma_1^{1R} T_2} \frac{\partial}{\partial y} (\bar{h}^0 e^{-2\gamma_1^{1R} T_2} + \epsilon^2 (e^{-2\gamma_1^{1R} (T_2 - T_1)} \bar{h}^1 + \bar{h}^2))$$

In general, we find for $\ell \geq 1$ that

$$\Phi^{\ell+1} \sim e^{2\gamma_1^{\ell R} T_\ell} \frac{\partial}{\partial y} (\bar{h}^0 e^{-2\gamma_1^{\ell R} T_\ell} + \epsilon^2 \sum_{k=1}^{\ell} e^{-2(\gamma_1^{\ell R} T_\ell - \gamma_1^{k R} T_k)} \bar{h}^k)$$

which is an approximate expression of the eddy memory. The memory arises here because of the successive corrections of the mean state determine the instabilities and hence the thickness fluxes. With the assumption that the γ_1^{kR} do not vary much, we can take $r = 1/(2\gamma_1^{1R})$ and the memory function can be approximated as

$$\kappa_1(T - T') = e^{-(T - T')/r}$$

where r measures the memory strength which is the same as in the previous section. The memory strength depends directly on the growth rate of the instability at criticality which in turn is affected by the zonal background state.

5 Summary and discussion

In this paper, we provided a specific example of the weakly nonlinear eddy-memory effect [12] through an analysis of the stability of a zonal jet in a two-layer quasi-geostrophic model. For the case that the background linear friction is high enough such that the $k = 0$ mode is damped, the jet becomes unstable for a certain value of the control parameter μ_c at a critical value k_c . Due to the instability, an eastward propagating traveling wave packet is amplified and the (in general complex) amplitude A of the envelope of this wave packet can be determined from a Ginzburg–Landau equation. To explain the eddy memory in the thickness flux, we focus on the Stokes solution of the Ginzburg–Landau equation which is spatially homogeneous.

When the background wind stress varies in time, we showed (under several approximations) that the memory kernel in the thickness flux (when related to the forcing variation) is a decaying exponential and the memory timescale is inversely proportional to the growth factor of the instability. The explicit form of the kernel is obtained under the approximation that the instability growth

and the associated spatial patterns do not vary much with the forcing (because both k_c and μ_c do not vary much) and that most of the variation is controlled by the nonlinear term in the Ginzburg–Landau equation.

When there are no external variations in the wind-stress forcing, the eddy-memory in the thickness flux–background state relation is caused by successive modification of the background state that lead to modifications of the instabilities on this background state. In the frame of the traveling waves, the self-interaction of this wave packet produces a correction to the background flow. The amplitude of this correction is determined by a Ginzburg–Landau equation and develops over a much longer timescale than the oscillatory part of the instability. Hence, the eventual eddy-thickness flux depends on the slow development of the background state generated by successive self-interactions of the instability.

In all these results, we kept the distance between the parameter value and the critical value constant, although the critical value slightly varies with the background state. While this is not important for the explanation of the exponential memory kernel here, it may lead to an oscillatory component in kernel function when the mean state adjustment is such that it first amplifies and then damps the growth of perturbations. We also did not consider non-normal growth of the perturbations, which in principle could also contribute to the eddy memory.

The memory kernel result can in principle also be obtained by linear response theory [26, 27] where the equilibrium attractor is just the zonal background jet state at criticality. This method can actually also be used to study the memory in a full statistical equilibrium state and hence can shed light on what memory is caused by eddy–eddy interactions [12]. The presence of eddy memory in the ocean may also lead to more detailed explanations on low-frequency variability phenomena in ocean models, such as the turbulent oscillator [9] in the midlatitude gyres and the Southern Ocean Mode [11] and we hope that this paper will stimulate work in this direction.

Acknowledgements HD thanks the Kavli Institute for Theoretical Physics and the University of California at Santa Barbara for their hospitality and excellent working facilities during November–December 2021. This research was supported in part by the National Science Foundation under Grant No. NSF PHY-1748958. GEM was funded by the United States National Science Foundation grant OCE-1829969.

Data Availability Statement The (Fortran) code for computing the coefficients in the GLE for the two-layer model is available on GitHub (<https://github.com/hadijkstra/EJP-Plus-EM>).

Open Access This article is licensed under a Creative Commons Attribution 4.0 International License, which permits use, sharing, adaptation, distribution and reproduction in any medium or format, as long as you give appropriate credit to the original author(s) and the source, provide a link to the Creative Commons licence, and indicate if changes were made. The images or other third party material in this article are included in the article's Creative Commons licence, unless indicated otherwise in a credit line to the material. If material is not included in the article's Creative Commons licence and your intended use is not permitted by statutory regulation or exceeds the permitted use, you will need to obtain permission directly from the copyright holder. To view a copy of this licence, visit <http://creativecommons.org/licenses/by/4.0/>.

Appendix: Derivation of the Ginzburg–Landau equation

This derivation is fairly standard and was already presented in detail in [25], but is repeated here for convenience. The equations of the linear stability analysis were determined at $\mathcal{O}(\epsilon E)$. At a next order $\mathcal{O}(\epsilon^2 E)$, the equations are

$$(i\omega_c \hat{\mathcal{M}}(k_c) + \hat{\mathcal{L}}(k_c))\Phi^{(12)} = -(i\omega_c \hat{\mathcal{M}}_k(k_c) + \hat{\mathcal{L}}_k(k_c) - c_g \hat{\mathcal{M}}(k_c)) \frac{\partial \Phi^{(11)}}{\partial X} \quad (48)$$

where the subscript k indicates differentiation to k . At $\mathcal{O}(\epsilon^2)$ and $\mathcal{O}(\epsilon^2 E^2)$, one finds

$$\hat{\mathcal{L}}(0)\Phi^{(02)} = -2\mathcal{R}(\mathcal{N}(\Phi^{(11)})\Phi^{(11)*}) \quad (49a)$$

$$(2i\omega_c \hat{\mathcal{M}}(2ik_c) + \hat{\mathcal{L}}(2ik_c))\Phi^{(22)} = -\mathcal{N}(\Phi^{(11)})\Phi^{(11)} \quad (49b)$$

where \mathcal{R} indicates real part and $*$ again complex conjugate. Using the relation $\Phi^{(11)} = A(X, T)\Psi$ in the Eqs. (48) and (49b) leads to

$$\Phi^{(12)} = \frac{\partial A}{\partial X} \Psi^{(12)}; \quad \Phi^{(02)} = |A|^2 \Psi^{(02)}; \quad \Phi^{(22)} = A^2 \Psi^{(22)} \quad (50)$$

where the vectors $\Psi^{(12)}$, $\Psi^{(02)}$ and $\Psi^{(22)}$ satisfy

$$(i\omega_c \hat{\mathcal{M}}(k_c) + \hat{\mathcal{L}}(k_c))\Psi^{(12)} = -(i\omega_c \hat{\mathcal{M}}_k(k_c) + \hat{\mathcal{L}}_k(k_c) - c_g \hat{\mathcal{M}}(k_c))\Psi \quad (51a)$$

$$\hat{\mathcal{L}}(0)\Psi^{(02)} = -2\mathcal{R}(\mathcal{N}(\Psi)\Psi^*) \quad (51b)$$

$$(2i\omega_c \hat{\mathcal{M}}(2ik_c) + \hat{\mathcal{L}}(2ik_c))\Psi^{(22)} = -\mathcal{N}(\Psi)\Psi \quad (51c)$$

and these equations are complemented with the appropriate boundary conditions at each order of the expansion.

Differentiation of the eigenvalue problem (14) to k and use of the group velocity at criticality gives $\Psi^{(12)}$ from (51a) as

$$\Psi^{(12)} = -i \frac{\partial \Psi}{\partial k} \tag{52}$$

evaluated at criticality. The left-hand sides of (51b, c) are non-singular and hence can be solved for $\Psi^{(02)}$ and $\Psi^{(22)}$. At $\mathcal{O}(\epsilon^3 E^2)$, a singular problem is obtained for $\Psi^{(13)}$, i.e.,

$$(i\omega_c \hat{\mathcal{M}}(k_c) + \hat{\mathcal{L}}(k_c))\Psi^{(13)} = -(\mathcal{M}(k_c)\Psi \frac{\partial A}{\partial T} + m\Gamma A + \Sigma \frac{\partial^2 A}{\partial X^2} + \Lambda A|A|^2) \tag{53}$$

where

$$\Gamma = (\hat{\mathcal{L}}_\mu(k_c) - i\omega_c \hat{\mathcal{M}}_\mu(k_c))\Psi \tag{54a}$$

$$\begin{aligned} \Sigma = & \frac{1}{2}(i\omega_c \hat{\mathcal{M}}_{kk}(k_c) - \hat{\mathcal{L}}_{kk}(k_c) - 2c_g \hat{\mathcal{M}}_k(k_c))\Psi \\ & + i(i\omega_c \hat{\mathcal{M}}_k(k_c) - c_g \hat{\mathcal{M}}(k_c) - \hat{\mathcal{L}}_k(k_c))\Psi_k \end{aligned} \tag{54b}$$

$$\Lambda = \mathcal{N}(\Psi)\Psi^{(02)} + \mathcal{N}(\Psi^{(02)})\Psi + \mathcal{N}(\Psi^{(22)})\Psi^* + \mathcal{N}(\Psi^*)\Psi^{(22)} \tag{54c}$$

In general, the right-hand side of (53) is not contained in the range of the linear operator on the left-hand side. Since the kernel of the operator $i\omega_c \hat{\mathcal{M}}(k_c) + \hat{\mathcal{L}}(k_c)$ has dimension 1, it is spanned by one vector, here indicated by Ω ; this implies that

$$\Omega^H (i\omega_c \hat{\mathcal{M}}(k_c) + \hat{\mathcal{L}}(k_c))\mathbf{W} = 0 \tag{55}$$

where \mathbf{W} is the right-hand side of (53) and the superscript H indicates Hermitian transposed. The resulting amplitude equation from (53) becomes the Ginzburg–Landau equation

$$\frac{\partial A}{\partial T} = \gamma_1 A + \gamma_2 \frac{\partial^2 A}{\partial X^2} - \gamma_3 A|A|^2 \tag{56}$$

with

$$\gamma_1 = m \frac{\Omega^H \Gamma}{\Omega^H \hat{\mathcal{M}}(k_c)\Psi} ; \quad \gamma_2 = \frac{\Omega^H \Sigma}{\Omega^H \hat{\mathcal{M}}(k_c)\Psi} ; \quad \gamma_3 = -\frac{\Omega^H \Lambda}{\Omega^H \hat{\mathcal{M}}(k_c)\Psi} . \tag{57}$$

References

1. B. Fox-Kemper, A. Adcroft, C.W. Böning, E.P. Chassignet, E. Curchitser, G. Danabasoglu, C. Eden, M.H. England, R. Gerdes, R.J. Greatbatch, S.M. Griffies, R.W. Hallberg, E. Hanert, P. Heimbach, H.T. Hewitt, C.N. Hill, Y. Komuro, S. Legg, J.L. Sommer, S. Masina, S.J. Marsland, S.G. Penny, F. Qiao, T.D. Ringler, A.M. Treguier, H. Tsujino, P. Uotila, S.G. Yeager, Challenges and prospects in ocean circulation models. *Front. Mar. Sci.* **6**, 65 (2019). <https://doi.org/10.3389/fmars.2019.00065>
2. A. Jüling, A. Heydt, v d, H. A. Dijkstra, Effects of strongly eddying oceans on multidecadal climate variability in the Community Earth System Model. *Ocean Sci.* **17**, 1251–1271 (2021). <https://doi.org/10.5194/os-17-1251-2021>
3. R.D. Smith, M.E. Maltrud, F.O. Bryan, M.W. Hecht, Numerical simulation of the North Atlantic Ocean at 0.1 degree resolution. *J. Phys. Oceanogr.* **30**, 1532–1561 (2000)
4. H.A. Dijkstra, P.C.F. Van der Vaart, On the physics of upgradient momentum transport in unstable eastward jets. *Geophys. Astrophys. Fluid Dyn.* **88**, 295–323 (1998)
5. P.R. Gent, J.C. McWilliams, Isopycnal mixing in ocean circulation models. *J. Phys. Oceanogr.* **20**, 150–155 (1990)
6. W.R. Young, An exact thickness-weighted average formulation of the Boussinesq equations. *J. Phys. Oceanogr.* **42**, 692–707 (2012). <https://doi.org/10.1175/jpo-d-11-0102.1>
7. P.R. Gent, The Gent–McWilliams parameterization: 20/20 hindsight. *Ocean Model.* **39**, 2–9. <https://doi.org/10.1016/j.ocemod.2010.08.002>, <https://www.sciencedirect.com/science/article/pii/S1463500310001253>. modelling and Understanding the Ocean Mesoscale and Submesoscale (2011)
8. A. Sinha, R.P. Abernathy, Time scales of Southern Ocean eddy equilibration. *J. Phys. Oceanogr.* **46**, 2785–2805 (2016)
9. P.S. Berloff, A.M. Hogg, W.K. Dewar, The turbulent oscillator: a mechanism of low-frequency variability of the wind-driven ocean gyres. *J. Phys. Oceanogr.* **37**, 2362–2386 (2007)
10. A.M.C. Hogg, J.R. Blundell, Interdecadal variability of the southern ocean. *J. Phys. Oceanogr.* **36**, 1626–1645 (2006). <https://doi.org/10.1175/JPO2934.1>
11. D. Le Bars, J.P. Viebahn, H.A. Dijkstra, A Southern Ocean mode of multidecadal variability. *Geophys. Res. Lett.* **43**, 1–9 (2016)
12. G.E. Manucharyan, A.F. Thompson, M.A. Spall, Eddy memory mode of multidecadal variability in residual-mean ocean circulations with application to the Beaufort Gyre. *J. Phys. Oceanogr.* **47**, 855–866 (2017)
13. A. Jüling, H.A. Dijkstra, A.M. Hogg, W. Moon, Multidecadal variability in the climate system: phenomena and mechanisms. *Eur. Phys. J. Plus* **135**, 506 (2020). <https://doi.org/10.1140/epjp/s13360-020-00515-4>
14. J. Viebahn, H. A. Dijkstra, D. C, Toward a turbulence closure based on energy modes. *J. Phys. Oceanogr.* **49**, 1075–1097 (2019). <https://doi.org/10.1175/jpo-d-18-0117.1>
15. S.K. Falkena, C. Quinn, J. Sieber, J. Frank, H.A. Dijkstra, Derivation of delay equation climate models using the Mori–Zwanzig formalism. *Proc. R. Soc. A* **475**, 20190075 (2019)
16. J. Wouters, V. Lucarini, Multi-level dynamical systems: connecting the ruelle response theory and the Mori–Zwanzig approach. *J. Stat. Phys.* **151**, 850–860 (2013). <https://doi.org/10.1007/s10955-013-0726-8>

17. W. Moon, G.E. Manucharyan, H.A. Dijkstra, Eddy memory as an explanation of intraseasonal periodic behaviour in baroclinic eddies. *Q. J. R. Meteorol. Soc.* **147**, 2395–2408 (2021). <https://doi.org/10.1002/qj.4030>
18. W. Moon, G.E. Manucharyan, H.A. Dijkstra, Baroclinic instability and large-scale wave propagation on planetary-scale atmosphere. *Q. J. R. Meteorol. Soc.* **148**, 809–825 (2022)
19. E.T. Eady, Long waves and cyclone waves. *Tellus* **1**, 33–52 (1949)
20. N.A. Phillips, A simple three-dimensional model for the study of large-scale extratropical flow patterns. *J. Meteor.* **8**, 381–394 (1951)
21. A. F. Lovegrove, I. M. Moroz, P. L. Read, Bifurcations and instabilities in rotating, two-layer fluids: II. β -Plane. *Nonlinear Process. Geophys.* **9**, 289–309 (2002). <https://doi.org/10.5194/npg-9-289-2002>
22. J. Pedlosky, Finite-amplitude baroclinic waves. *J. Atmos. Sci.* **27**, 15–30 (1970). [https://doi.org/10.1175/1520-0469\(1970\)027<0015:FABW>2.0.CO;2](https://doi.org/10.1175/1520-0469(1970)027<0015:FABW>2.0.CO;2)
23. R.D. Romea, The effects of friction and β on finite amplitude baroclinic waves. *J. Atmos. Sci.* **34**, 1689–1695 (1977)
24. P. Welander, A two-layer frictional model of wind-driven motion in a rectangular oceanic basin. *Tellus* **18**, 54–62 (1966). <https://doi.org/10.3402/tellusa.v18i1.9183>
25. P.C.F. Van der Vaart, H.A. Dijkstra, Sideband instabilities of mixed barotropic/baroclinic waves growing on a midlatitude zonal jet. *Phys. Fluids* **9**, 615–631 (1997)
26. V. Lucarini, Response operators for Markov processes in a finite state space: radius of convergence and link to the response theory for axiom a systems. *J. Stat. Phys.* **162**, 312–333 (2016). <https://doi.org/10.1007/s10955-015-1409-4>
27. D. Ruelle, A review of linear response theory for general differentiable dynamical systems. *Nonlinearity* **22**, 855–870 (2009). <https://doi.org/10.1088/0951-7715/22/4/009>